

The Unreasonable Effectiveness of Contact Tracing on Networks with Cliques

Abbas K. Rizi,¹ Leah A. Keating,² James P. Gleeson,² David J.P. O’Sullivan,² and Mikko Kivelä¹

¹*Department of Computer Science, School of Science, Aalto University, FI-00076, Finland*

²*MACSI, Department of Mathematics and Statistics,
University of Limerick, Limerick, V94 T9PX, Ireland*

(Dated: April 21, 2023)

Contact tracing, the practice of isolating individuals who have been in contact with infected individuals, is an effective and practical way of containing disease spread. Here, we show that this strategy is particularly effective in the presence of social groups: Once the disease enters a group, contact tracing not only cuts direct infection paths but can also pre-emptively quarantine group members such that it will cut indirect spreading routes. We show these results by using a deliberately stylized model that allows us to isolate the effect of contact tracing within the clique structure of the network where the contagion is spreading. This will enable us to derive mean-field approximations and epidemic thresholds to demonstrate the efficiency of contact tracing in social networks with small groups. This analysis shows that contact tracing in networks with groups is more efficient the larger the groups are. We show how these results can be understood by approximating the combination of disease spreading and contact tracing with a complex contagion process where every failed infection attempt will lead to a lower infection probability in the next attempts. Our results illustrate how contact tracing in real-world settings can be more efficient than predicted by models that treat the system as fully mixed or the network structure as locally tree-like.

Testing, contact tracing, and isolating are effective procedures to control the spread of diseases and prevent outbreaks. During the COVID-19 pandemic, this methodology was adopted globally, with varying levels of success [1]. Countries like China, South Korea and Singapore have implemented successful programs [2], while the United Kingdom [3] and the United States have struggled with implementing effective programs [2, 4]. Although contact tracing is a more targeted method than blanket measures such as school closures and travel restrictions, which result in significant monetary and societal costs [5], implementing contact tracing programs still comes with significant costs. In addition, unlike other measures, contact tracing relying on digital tracking systems can lead to privacy concerns related to digital surveillance in the context of automated contact tracing methods [2]. Therefore, it is crucial to carefully evaluate the costs and benefits before implementing any contact tracing measures on a widespread scale.

The efficacy of contact tracing is commonly evaluated based on the proportion of infected individuals placed in quarantine and its effect on onward transmission chains, which are disrupted as a result [4, 6]. The standard methodology behind this evaluation relies on the assumption that the contact network is locally structured as a tree. However, social networks are not tree-like but are comprised of various overlapping groups such as families, workplaces, and other communities.

When an individual is infected in a social group, they infect a subset of the group, and contact tracing isolates another subset. Typically, contact tracing is considered effective only for the overlapping part of these subsets, i.e., individuals who are both isolated and infected, as this can break direct transmission chains. However, isolating people in the group who did not get the infection from the initially infected individual is likely to be bene-

ficial to the control of the spread of the contagion. Suppose the contact tracing did not work perfectly. In that case, there can be individuals in the group who continue infecting others, and isolating people in the group comes exactly at the right time and place. Thus, even seemingly unnecessary isolations caused by contact tracing may still have a positive impact.

We demonstrate the group dynamics of contact tracing and their effect on outbreak sizes and the epidemic threshold by developing a stylized contact tracing model and a random network model with cliques. This allows us to build on methods developed for spreading processes in networks with cliques [7–9]. In order to investigate the sole impact of group structure, we aim to compare network results in which nodes possess an equal number of connections but belong to groups of different sizes. This means we are analyzing homogeneous networks in our model, where nodes have equivalent link numbers and network clustering, except for the variation in clustering between the networks being studied. This allows us to isolate the effect of clustering on contact-traced epidemics. Our model suggests that clique structure would have a minor effect on a typical SIR spreading process without contact tracing. However, our findings also indicate that the presence of group structure would enhance the effectiveness of contact tracing, intensifying the impact of cliques. Specifically, contact tracing in a network with cliques has a non-linear impact on the efficiency of halting the spread of chains that occur over a single link. This contrasts with models that assume a locally tree-like contact structure.

Social networks often exhibit a complex and dense structure that deviates from a tree-like topology, particularly in the context of disease spreading. This deviation can be attributed to the high clustering observed in families, workplaces, schools, and other social foci [10, 11].

Clique structures are particularly important in complex contagion-type spreading processes [12, 13]. These processes are typically used to model the spreading of behavior in social networks where adoption of behavior becomes more likely after previous exposures [14]. This contrasts with disease-spreading models, where infections are always treated as independent of previous exposures. We show that the combination of disease spreading and contact tracing can be approximated as a complex contagion process, where repeated exposures reduce the probability of infection because they can lead to isolation and thus can make the subsequent infections impossible. This interpretation of contact tracing as complex contagion explains our results on the importance of group structure.

The rest of this paper is organized as follows. In Section I, we will introduce the random network structure, the epidemic model, and the contact tracing procedure. In Section II, we will find the epidemic threshold for networks with cliques. We will show how multi-type branching processes based on motifs [12] can be used to derive mean-field solutions to this problem. Finally, we show our results based on this approach. In Section III, we introduce the complex contagion approximation of the process. We show that contact tracing on networks with cliques can be approximated as a complex contagion process.

I. NETWORK STRUCTURE & THE SPREADING PROCESS

A. Random Network Models with Cliques

Numerous studies have demonstrated that to model the efficacy of pharmaceutical and non-pharmaceutical interventions in the context of an epidemic, it is essential to consider the network structure and various health behaviors of the population in which the disease is spreading [15, 16]. Societies are interconnected in distinct ways, implying that a strategy that works well in one place may not be effective in another. Therefore, it is crucial to carefully assess the effectiveness of interventions, considering the impact of social interactions on the spread of the targeted disease.

Here, we want to investigate the sole effect of social groups on contact tracing. In studying epidemic processes, cliques are the most straightforward choice to represent social groups in contact networks. In social networks, c -cliques are complete subgraphs representing a group of c people who are all connected and, thus, can directly infect each other [7, 8]. Clique structure breaks the tree-like assumption, which aligns with empirical findings on social networks [17].

To generate networks of size N , we can use a configuration model with a prescribed clique structure with two sets of node types — defining a bipartite network. Initially, the graph is divided into two groups (a node group

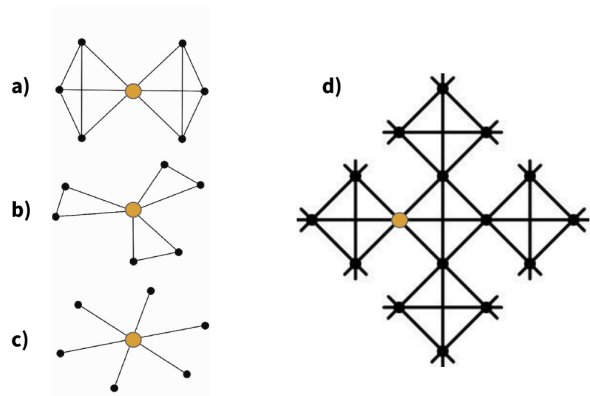


FIG. 1. Schematic of 6-regular c -clique networks. Panels (a-c) display the neighborhoods around a (highlighted) node in 4, 3 and 2-clique networks. These patterns repeat around every node in the random networks. (d) Part of the local neighborhood of a 4-clique network, i.e., an extended neighborhood around the panel (a). Note that every node has degree 6, and we only show link stubs for every of the nodes. This is the expected local pattern in a very large clique network.

and a clique group). As this is a bipartite graph, there can only be links between the nodes and clique groups. We give each member of the node group r stubs and each member of the clique group c stubs. As there are a total of N nodes, each with degree r , the total number of stubs in the node group is $N \times r$. The total number of stubs in the clique group must be the same. Therefore, the clique group will have $(N \times r)/c$ members. We connect, at random, stubs in the node group to stubs in the clique group. This provides a network that defines which nodes are connected to the same clique. Thus, by taking the node projection of the bipartite network, we can obtain the desired network structure — by connecting any nodes that share a connection to the clique group. In the thermodynamic limit, such contact networks have a vanishingly small number of self-loops or multi-links. See [18, 19] for further details on these network structures. In practice, when we build such networks for our simulations, we remove self-loops and multi-links, ending up with a simple graph. Then, each c -clique contributes $c - 1$ links to a node degree. Therefore, the number of cliques that a node is a part of, n_c , satisfies the condition $n_c(c - 1) = r$, see Fig. 1. When $c = 2$, the model generates a random r -regular graph.

B. Spreading Processes on Networks

Spreading processes on networks with cliques, including the networks described above, have been studied in the literature. A typical approach is to take advantage of the connection between the paradigmatic Susceptible-Infectious-Recovered (SIR) processes and the connectivity of the networks after random link removal, which can be analyzed within the framework of percolation the-

ory [20–22]. That is, under specific assumptions, certain spreading processes can be mapped to a percolation problem. The epidemic properties, such as the epidemic threshold and the final outbreak size, can be read from the percolation threshold and the size of the giant component, respectively [16, 20].

It is worthwhile to note that clustering alone does not determine how the epidemic threshold [23] or the component size distribution of that network would change. Poisson-clustered networks, where the sizes of the cliques are sampled from a Poisson distribution, can decrease the critical link percolation threshold while reducing the maximum size of the giant component [17, 24]. However, we can show that clustering may increase the critical threshold in other settings while not always reducing the size of the giant component [25–29]. In the cases of not adding cliques but other clustered subgraphs to a network, by increasing the clustering, the size of the giant component and the critical threshold do not necessarily increase or decrease [30, 31]. Moreover, in some cases, such as Poisson-clustered networks with a high average degree, clustering may have negligible effects on network dynamics [9, 32, 33].

This work focuses on a SIR process combined with contact tracing on random networks with cliques. It is good to bear in mind that in the absence of contact tracing, our general approach reduces to the typical SIR analysis on networks with cliques.

C. SIR+Q Dynamics & Outbreak Size

Both contact tracing and disease transmission in real social systems are complicated processes. We aim to reduce these complications into a minimally mathematically tractable model that captures the most important dynamics of contact tracing and disease spreading. We employ a discrete-time SIR model to model disease dynamics [34], where at each time step, the infected (I) individuals infect neighboring susceptible nodes (S) with *transmission* probability p . After this, the infected individuals are moved to the recovered (R) compartment. Importantly, this time-discretized model ignores variations in recovery times and can only implicitly consider complications such as incubation periods [35]. These dynamics strike an ideal balance between realism and simplicity for this work. Contact tracing can be implemented in various ways, such as with phone applications [15], in different manual tracing settings, or with combinations of these two [36]. The success of contact tracing can be affected by the ability of individuals to recall contacts, the delay times in the tracing process, mobile-phone application adoption, and the extent to which the individuals follow the isolation recommendations. We model all these complications with the *isolation* probability α of a neighboring node successfully isolating such that all further infections are avoided. Further, the isolations are done independently using the same contact network

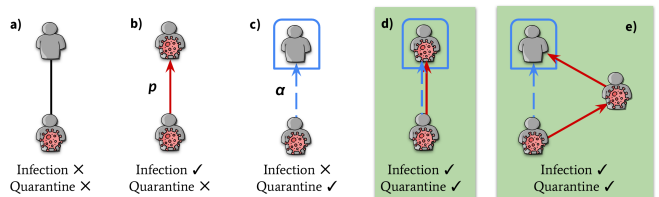


FIG. 2. Schematic of contact tracing and spreading without loops (a-d) and with local loops (e). Infections that would be successful are marked with solid red links and successful contact tracing with dashed blue links. After each exposure, a susceptible node (S) isolates itself with probability α and gets infected with probability p , independently. If no loops are considered, the combination of infections and contact tracing can be reduced to a single link, and there are four possible scenarios: (a) nothing happens, (b) the infection spreads to the neighbor, but contact tracing fails, (c) the infection fails to spread, but contact tracing succeeds, or (d) both infections spreads and the contact tracing succeeds. The last case, highlighted with a green background, is the only one where contact tracing makes a difference in a tree-like model during the early stages of the epidemic. (e) In the presence of local loops, the scenario shown in panel (c) can become beneficial, because an infection through a common neighbor of both nodes can be avoided. That is, as the quarantine takes place close to the infection, it can prevent the infection arriving to the neighbor through a local loop.

as the infections. In the model, this translates to infected nodes placing the neighboring susceptible nodes into compartment Q with probability α . Note that we do not explicitly keep track of the infection status of the quarantined nodes, but the nodes in the Q compartment can be either infected (Q_I) or susceptible (Q_S). See Fig. 2 for an illustration of the process.

We focus on contact tracing when the disease does not reach a significant part of the population. If the number of infected people grows large, contact tracing can become prohibitively expensive and render it ineffective as the delay times grow [37]. As our contact networks are large random graphs with cliques (see Sec. IA), the infection paths will not form significant long loops. This means that for our model, we can assume that the isolation times are long enough that they will stop all the incoming infections to a node, and we can simply keep the isolated nodes in the Q compartment indefinitely.

We assume the infection and contact tracing processes are independent (i.e., we treat p and α as independent probabilities). The order in which they are evaluated in the discrete-time model does not make a difference for the epidemic threshold. However, there is a slight variation in the epidemic size depending on the order, as the number of isolated individuals that are infected is affected by the order. For the epidemic size computations, we follow an order where we go through one infected-susceptible link at a time. First, we evaluate the epidemic spreading and then the contact tracing for that link. This way, the number of infected people in quarantine can be computed as $N_{Q_I} = pN_Q$. We find the size of an epidemic E by

summing up the number of infected people in and out of quarantine, N_{Q_I} and N_R , respectively.

By simulating the dynamics, we observe a sharp increase in the outbreak size from a small number of individuals being infected to a significant proportion of the network being infected once particular values of p and α are crossed. We accomplish this in our simulations by building large networks (with $N \approx 10^5$ nodes) according to Sec. IA, running the SIR+Q dynamics on them several times, and finding the ensemble average of the number of nodes in the different compartments in each run as our proxy of spreading statistics. The size of the outbreak is then given by the ensemble averages of the number of people in the R and Q_I compartments for each value of p and α . Fig. 3(a-c) illustrate the dependence of outbreak size on the value of p under different scenarios, namely in the absence of contact tracing ($\alpha = 0$), and with contact tracing at $\alpha = 0.25$ and $\alpha = 0.5$, for networks consisting of 2, 3, and 4-cliques. The outbreak size decreases for any given transmission probability as the clique size increases. Moreover, this effect is magnified by an increase in the value of α . Furthermore, we use the fluctuations in the outbreak sizes for determining the epidemic thresholds as described in detail in Sec. IIB1 and illustrated in Fig. 3b.

We will revisit the outbreak size in Sec. IIB3, and provide analytical calculations. The outbreak size in the sub-critical regime does not scale with the network size and also decreases dramatically by increasing α , as shown later in Fig. 9. Another potential approach to determine the outbreak size in such cases is through message passing methods [38]. Nonetheless, our primary focus in this study is on examining the impact of contact tracing on the epidemic threshold in networks with cliques. We will present two different approaches to calculating the epidemic thresholds in the upcoming sections, one based on a mean-field approach and one based on a complex contagion approximation to contact tracing.

II. EPIDEMIC THRESHOLD

A. Random Tree-like Networks

Given a population in a demographic steady state, with no history of a given infection or introduction of any intervention, the basic reproduction number R_0 determines if the introduction of the infectious agent causes an outbreak ($R_0 > 1$) or not ($R_0 < 1$) in the absence of interventions [39]. Therefore, R_0 as a threshold for the stability of a disease-free equilibrium in a compartmental model divides the phase space into super/sub-critical regions, respectively. When interventions such as contact tracing are implemented, we use the term “effective reproduction number” R_e instead of the “basic” reproduction number to differentiate between situations with no interventions in this paper. Therefore, to determine if the epidemic dies out or yields an outbreak in the pres-

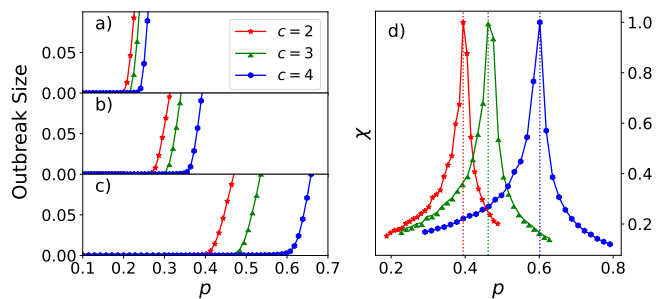


FIG. 3. Phase transitions from a disease-free equilibrium to an endemic state for 2, 3, and 4-clique networks with degree 6 as introduced in Sec. IA. (a-c) The outbreak size E , normalized to the network size, is shown on the vertical axis for when (a) $\alpha = 0$ (no contact tracing), (b) $\alpha = 0.25$, and (c) $\alpha = 0.5$, from top to bottom respectively. Note that the transition points are shifted slightly to the right for larger clique sizes, c , even when there is no contact tracing ($\alpha = 0$), but this difference is substantially amplified for larger α values. (d) The coefficient of variation of outbreak sizes in an ensemble, χ normalized to unity for $\alpha = 0.5$. We use χ to numerically detect the transition point as it peaks at the epidemic threshold. Results are based on Monte Carlo simulations introduced in Sec. IC and Sec. IIB1.

ence of intervention, we need to compute the value of R_e [16]. R_e as a bifurcation parameter in our epidemic model depends on the spreading parameters, p and α , and the network structure, which is determined by c and r . When $R_e = 1$, each *active* (infected non-isolated) node infects, on average, one node that does not isolate.

For a large tree-like network, like a random r -regular graph in Fig. 1c, we can find the epidemic threshold in the αp -plane using

$$R_e = p(1 - \alpha)\bar{d}, \quad (1)$$

and setting $R_e = 1$. Here \bar{d} is the expected excess degree of the network, which is the expected number of links a node that is reached by following a uniformly randomly chosen link has, not counting the link that was used to reach that node. As our networks have uniform degree distributions, such that every node has degree r , the expected excess degree is just the degree minus one, $\bar{d} = r - 1$. It should be noted that even in the case of the most severe disease with $p = 1$, it is still possible to avoid an outbreak. By setting $p = 1$ in Eq. 1 and solving for α , we can determine that if the quarantine is carried out in such a way that $\alpha > 1 - 1/\bar{d}$, the effective reproduction number, R_e , will remain below 1, and hence no outbreak will occur, provided that $\bar{d} > 1$.

In general, for a tree-like random network with expected excess degree \bar{d} , we can rewrite the effective reproduction number as a product of spreading properties and network structure as $R_e = p_e \bar{d}$ where p_e is the effective transmission probability and defined as

$$p_e = p(1 - \alpha). \quad (2)$$

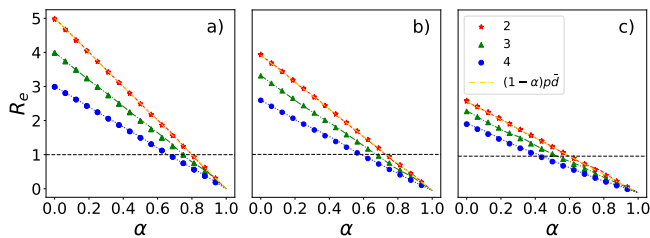


FIG. 4. How contact tracing on clique network reduces the effective reproduction number R_e by increasing α . Effective reproduction number for different networks with cliques with $r = 6$ for transmission probabilities (a) $p = 1.0$, (b) $p = 0.75$ and (c) $p = 0.5$. The dotted lines are from the mean-field calculations introduced in Sec. II B 2 and the markers are from Monte Carlo simulations described in Sec. II B 1. The yellow dashed lines, which overlap with the red curves with stars, represent Eq. 1, which match the cases where $c = 2$ (tree-like networks). The larger the transmission probability, the larger the differences between the curves of different networks with cliques. The larger the clique size, the less effort we need to quarantine people since networks with larger cliques reach $R_e = 1$ for lower values of α .

So every active node can, on average, infect $R_e = p_e \bar{d}$ new people who can propagate the disease, i.e., are not themselves quarantining. When contact tracing is not in place ($\alpha = 0$), the effective reproduction number reduces to the basic reproduction number, $R_0 = p \bar{d}$, and since we ignore variations in recovery time, the SIR dynamics can be mapped to a bond percolation problem, where p represents the link occupation probability and the size of the giant component corresponds to the final outbreak size [35, 40]. This mapping results in the epidemic threshold being equivalent to the percolation threshold, which occurs at $p_c = 1/\bar{d} = 0.2$ for a 6-regular graph. Thus, a phase transition is expected from a disease-free equilibrium to an endemic state, as depicted in Fig. 3. When $\alpha = 0.5$ for a 6-regular graph, the epidemic threshold occurs at $p = 0.4$, according to Eq.1. Our forthcoming explanation of simulation results of random networks with cliques shows that this equation aligns exceedingly well with $c = 2$ (no loops), as demonstrated in Fig. 4. If the tree-like assumption does not hold, for example, when $c > 2$, an alternative method is required to determine R_e . This is the focus of the following section.

B. Networks with Cliques

1. Simulations

When considering networks with cliques, the standard approach to finding the epidemic threshold using Eq. 1 is not feasible since it relies on the assumption of a locally tree-like structure. Even though cliques in networks violate this assumption, rendering the equation unusable, when looking at an ensemble of simulations, there will be

high variation in outbreaks sizes at the epidemic threshold due to the critical nature of this point [20, 41]. Therefore, to determine the epidemic threshold for the SIR dynamics outlined in Sec.I C, we run a set of simulations and measure the coefficient of variation of the outbreak sizes χ , which is the ratio of the standard deviation of outbreak sizes to their ensemble average, $\chi = \sigma_E / \langle E \rangle$ [34]. This measurement captures the fluctuations in outbreak sizes and is an effective tool for identifying transition points since it typically displays a peak even in finite systems. The measure χ is analogous to susceptibility in the field of critical phenomena, which measures the response magnitude generated by a small external field disturbance [42]. When computed as a function of infection probability p , the peaks in χ indicate the epidemic thresholds for some value of α . Fig. 3d shows these curves for different networks with cliques; the larger the clique size, the larger the critical transmission probability. It shows that for a fixed r , here 6, contact tracing on networks with cliques is more effective when the contact networks include larger cliques.

When infected people are placed in the quarantine compartment, they cannot cause new infections in the next step. So, to find R_e in our simulations, we run our discrete-time dynamics and count, on average, how many people have been infected in each time step by a typical infected node. In different trials, we start with a single infected node, chosen uniformly at random in the network and follow how many susceptible nodes it infects, even if the contact tracing succeeds, such as the case in Fig. 2d. The total number of new infections caused by the seed node would be *individual* reproduction number of that node, and we report it as the effective reproduction number of generation $t = 1$. In the next step, we do the same for the resultant active (infected but not in quarantine) nodes generated by the seed node, one-after-another. Notice that from this step on, a neighbor of an active node may be in quarantine because of its interaction with other neighbors, not with the one it is receiving the infection from, such as the case e in Fig. 2. In these cases, the active node cannot infect the node which has been in quarantine via other nodes. When we are done with all the active nodes of this generation, we report the average number of individual reproduction numbers of these nodes as the effective reproduction at generation $t = 2$. The process can be continued for more generations, depending on the size of the network. For large enough networks, the ensemble average of effective reproduction number over different trials starts to stabilize from generation $t = 3$ in our simulations, indicating that its value remains constant for some time, depending on the network's size. Hence, we consider this stabilized value at $t = 3$ as the effective reproduction number R_e . For finite networks, this means that we need to run the simulation long enough for the process to stabilize but short enough that the ratio of the infected nodes to the network size remains close to zero. If no new infection happens in a generation, it means the disease has died

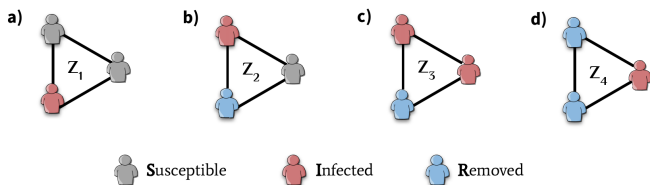


FIG. 5. Each 3-clique can have four life stages or diffusion patterns with at least one infected node in it. In Section II B 2, we consider both recovered and quarantined nodes to be in the R compartment. Using a 6-regular 3-clique network, we observe that a Z_1 node can form a Z_2 motif with two Z_1 nodes and a Z_3 motif with four Z_1 nodes. Additionally, a Z_2 node can create a Z_4 motif with two Z_1 nodes. Nodes in the Z_1 , Z_2 , and Z_4 motifs can transition to an infection-annihilated states such as $\{R, S, S\}$ which are not shown here. In Section III, we assume that both quarantined and susceptible nodes are in the S compartment, while only recovered individuals are in the R compartment.

out.

In Fig. 4, the values of R_e for various clique sizes are presented under different transmission probabilities for networks with approximately 10^5 nodes. The figure shows that for some value of p there is an almost linear relationship between R_e and α , but the slope is less steep for larger cliques. For $c = 2$, the analytical results from Eq. 1 perfectly match the observations.

2. Mean-field Approximation

By representing our stylized SIR model using a multi-type branching process, we can go beyond simulations and derive the relationship between p , α and clique size c on the epidemic threshold. Regardless of the network structure, we can always average the expected number of new infections over all possible infected types from our multi-type branching process with the next-generation matrix [39]. To do this, we track the propagation of clique motifs in a network under the introduced dynamics and form the next-generation matrix \mathbf{M} for the number of motifs present in the network. The matrix \mathbf{M} is also known as the mean matrix or the population projection matrix [43] and its element m_{ij} gives the expected number of motifs of type i , Z_i that are created in the next time steps from a motif of type j , Z_j .

Fig. 5 shows the motifs corresponding to the four life stages of a 3-clique. We have combined the isolated and recovered nodes into a single R compartment in this representation. As for the epidemic threshold computations, these two compartments are equivalent. The \mathbf{M} matrix represents the transitions between these motifs. For example, the infected node in Z_1 can infect one or two neighbors, corresponding to motifs Z_2 and Z_3 . Further, new $n_c - 1$ new Z_1 motifs are produced every time such an infection takes place. That is, when Z_1 turns into Z_2 there are also $n_c - 1$ new Z_1 motifs, and when it turns

i, j	m_{ij}
1, 1	$4p(1 - \alpha)$
1, 2	$2p(1 - \alpha)$
2, 1	$2p(1 - \alpha)^2(1 - p)$
3, 1	$p^2(1 - \alpha)^2$
4, 1	$2\alpha p(1 - \alpha)$
4, 2	$p(1 - \alpha)$

TABLE I. Non-zero elements of the next-generation matrix $\mathbf{M}_{4 \times 4}$ for a 3-clique network. m_{ij} gives the expected number of Z_i cliques from a Z_j clique, as shown in Fig. 5.

into Z_2 there are $2n_c - 2$ new Z_1 motifs created.

Table I shows the non-zero elements of \mathbf{M} . For example, the transition from Z_2 to Z_4 takes place when contact tracing fails (with probability $1 - \alpha$) and the infection is successful (with probability p), which means that, in expectation, a single Z_2 motif produces $m_{42} = p(1 - \alpha)$ new Z_4 motifs. The motif Z_4 can also be produced when the infected node in Z_1 , puts one neighbor in quarantine (with probability α) and fails to do so for the neighbor and infects it instead (which happens with probability $p(1 - \alpha)$). As there are two ways of choosing the infected and isolated neighbor, the expected number of Z_4 motifs produced by the Z_1 motif is given by $m_{41} = 2\alpha[(1 - \alpha)p]$. The rest of the transitions are produced similarly by computing the probabilities of going from one motif to another. As described in Appendix C, we write general formulas for any transition and use this to automatically generate \mathbf{M} matrices for cliques of any desired size.

What is significant about the next-generation matrix is that its spectral radius (Perron root), or the largest modulus of the eigenvalues, yields the effective reproduction number [44, 45] such that

$$R_e = \rho(\mathbf{M}), \quad (3)$$

and, epidemic thresholds for any given clique network can be found for finding p and α such that $R_e = 1$. We give more detailed arguments about this identity in the Appendix B, and show that this definition aligns with the simulation results described in Sec.II B 1 (see Fig. 4).

Fig. 6a presents the phase diagram of the epidemic for various networks with cliques by drawing $R_e = 1$ curves in the αp -plane. These curves divide the plane into sub- and super-critical regions. In the sub-critical region, there is no possibility of an outbreak that scales with the network size. In contrast, in the super-critical region, there is a positive probability of such an outbreak upon infection. For networks with cliques, increasing the clique size enlarges the sub-critical region and shrinks the super-critical region. Note that even in the absence of contact tracing when $\alpha = 0$, including a clique structure in random graph models, raises the epidemic threshold slightly. However, this effect is amplified by contact tracing, which can be observed as an increased difference between the critical p values as α increases.

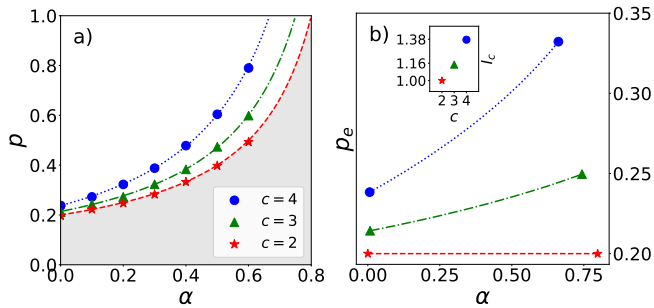


FIG. 6. Phase diagram showing that increasing the clique size increases the epidemic threshold and effectiveness of contact tracing. (a) The critical curves where $R_e = 1$ in the αp -plane for $c \in \{2, 3, 4\}$. The lines indicate results of the mean-field approximations as described in Sec. III and II A, and the markers show results for simulations described in Sec. II B 1. The shaded area is the sub-critical region for $c = 2$ where the infection eventually dies out after a finite number of generations for any clique size. (b) The same phase diagram in αp_e -plane, where $p_e = p(1 - \alpha)$ is the effective transmission probability defined in Eq. 2. The larger markers in the right end in panel b indicate extreme points from Eq. 4. The inset in panel b shows the relative maximum increase in the effective epidemic threshold for different networks with cliques. Each point in the inset is the ratio of the p_e values at the endpoints of each curve outside the inset, such that $I_c = p_e(\alpha_{\max})/p_e(\alpha_{\min})$.

We illustrate that the combined impact of contact tracing and cliques is larger than one would expect by the tree-like assumption by plotting the critical effective transmission probability p_e , defined in Eq.2, as a function of α . Fig. 6b displays this re-scaling of the critical values. For tree-like networks, such as 2-clique networks, $R_e = 1$ corresponds to a constant (horizontal line) in the re-scaled representation, while for networks with cliques, this value increases with α . This indicates that networks with cliques require much larger effective transmission probabilities to reach the epidemic threshold compared to what is expected by the tree-like approximation, with the difference growing as the isolation probability α increases. This shows the moderating effect that cliques structures can have on an epidemic in the presence of contact tracing, as it helps to cut not only onward infections but also indirect spreading paths in the network.

The transition points are strongly dependent on the node degree r , and while in Fig. 6 we kept the node degrees fixed to $r = 6$, it is important to note that the node degree r re-scales the transition points between sub- and super-critical. More precisely, if we use the excess degree to scale the critical p_e by plotting $(r - 1)p_e$ as a function of α , the phase diagram returns to a scale that is independent of r such that the $c = 2$ line is exactly at $(r - 1)p_e = 1$. This is illustrated for $r = 6$ and $r = 12$ in Fig. 6 and Fig. 7a, respectively. A more systematic exploration can be found in Fig. 7b, where each node belongs only to two cliques, $n_c = 2$, representing the ex-

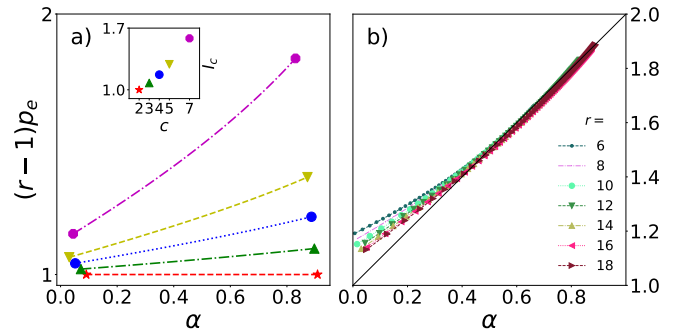


FIG. 7. Critical curves re-scaled as effective branching factors for tree-like networks $(r - 1)p_e$. Panel (a) is the same as panel Fig. 6b, but on the vertical axis, the effective transmission probabilities are multiplied by the excess degree. Further, results are shown for a larger network where $r = 12$. The red curves marked with stars are for the case that there $c = 2$ and the network is tree-like, therefore Eq. 1 holds such that $R_e = p_e d = p_e(r - 1) = 1$ for any α value. For $c > 2$, this equation does not hold. The right end markers on panel (a) indicate extreme points from Eq. 4. The inset shows the relative maximum increase in the effective epidemic threshold for different networks with cliques. Each point in the inset is the ratio of the p_e values at the endpoints of each curve outside the inset, such that $I_c = p_e(\alpha_{\max})/p_e(\alpha_{\min})$. (b) This panel shows how $(1 - r)p_e$ changes when we have networks with different degrees, $r = 6$ to $r = 18$, and maximal connectivity-preserving clique size (i.e., when $n_c = 2$).

treme non-trivial scenario where each clique is as large as possible without the network consisting solely of isolated cliques. In this case, the critical curves collapse in the re-scaled plot for a range of $r = 6$ to $r = 18$ that we tested. The collapse approximately follows a straight line from $(r - 1)p_e = 1$ for $\alpha = 0$ to $(r - 1)p_e = 2$ for $\alpha = 1$, with the approximation getting better for larger values of α . Note that for $\alpha = 0$, the critical transmission probability equals the critical bond percolation probability, as explained in Sec. I B and it can be obtained through analysis similar to Fig. 3.

The curve collapse can be understood by examining the extreme cases of (1) $\alpha = 0$ where there is no contact tracing; and (2) $p = 1$ where the infection always succeeds, and the critical point for contact tracing probability α is at its maximum. Let us start by determining the critical probability α required to prevent an outbreak when $p = 1$. In this case, infected nodes always infect all of their neighbors, and during the early stages of the epidemic, each clique either has (1) exactly one infected node and $c - 1$ susceptible nodes, (2) one recovered node and $c - 1$ infected nodes (out of which a fraction of α are isolated in expectation), or (3) only susceptible nodes. When an infection arrives at a clique, the infected node, which is not in quarantine, can spread the infection to $(n_c - 1)(c - 1)$ new nodes (offspring) in the next time step, as illustrated in Fig. 8. Therefore, α_c can be obtained by setting the expected number of active (infected but not in quarantine) nodes to one, which occurs when

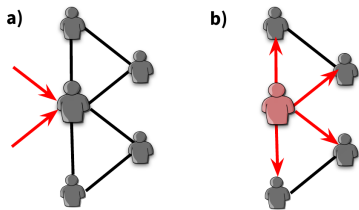


FIG. 8. Spreading process in a 6-regular 3-clique network under the extreme case of $p = 1$, where the infection propagates severely through the cliques. In this scenario, (a) an active node (infected but not in quarantine) can transmit the disease to other nodes in its adjacent cliques, (b) resulting in new infections. The number of new infections caused by an active node is not equal to the total number of members in the cliques that the node belongs to, which is $n_c(c - 1)$, but rather the number of members in the cliques attached to that node, excluding the clique that infection is coming from, which is $(n_c - 1)(c - 1) = 2 \times 2$. For further details on the network structure and spreading dynamics, refer to Sec. I.

$(1 - \alpha)(n_c - 1)(c - 1) = 1$. Therefore, the critical value for α is given by

$$\alpha_c = 1 - ((n_c - 1)(c - 1))^{-1}. \quad (4)$$

Substituting this into $p_e = 1 - \alpha$, gives

$$(r - 1)p_e = \frac{n_c(c - 1) - 1}{(n_c - 1)(c - 1)}. \quad (5)$$

Large markers in the right end of Fig. 6 shows such extreme points (α_c, p_c) . The critical transmission probability α approaches 1 when the clique size c grows to infinity. Using Eq. 5 this means that $(r - 1)p_e \xrightarrow{c \rightarrow \infty} \frac{n_c}{n_c - 1}$, which yields the value 2 when $n_c = 2$, for example. This explains why the re-scaled critical infection probability curves approach 2 when α is sufficiently large Fig. 7b.

3. Outbreak Size Revisited

The characterization of the process provides access to methods for calculating quantities of interest, such as the epidemic size, via the next-generation matrix. We are interested in the outbreak size (the expected total number of infected individuals in an outbreak) for a given parameter set. We follow closely the method outlined in Ref. [12], where they derived the expected epidemic size, E , in the sub-critical regime. We consider the contributions for subtrees seed of each motif type (\vec{z}) — as well as the expected number of offspring of each type from each motif type, which has already been discussed in Sec. II B 2 via the next-generation matrix. We also need to consider the number of infected nodes contributed by each type, which will be given by the vector \vec{I} . The expected epidemic size, E , can be found by solving the following two

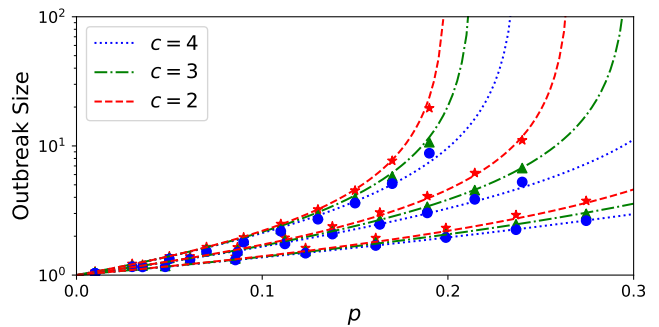


FIG. 9. Outbreak size in the sub-critical regime as a function of p across the three network structures, while taking into account the influence of isolation probability α . Nine curves are grouped into three sets (from left to right) according to their isolation probabilities, with each set containing three curves with $\alpha = 0.0, \alpha = 0.25$, and $\alpha = 0.5$. These groupings demonstrate the influence of α on outbreak size in the sub-critical regime. Increasing α or clique size reduces the outbreak size, as calculated by Eq.6 and Eq.7 using the next-generation matrix from mean-field approximation found in Sec. II B 2. Markers represent the results of 50,000 simulations, while dotted lines depict the results of the mean-field calculations presented in Sec. II B 3.

equations:

$$(\mathbf{I} - \mathbf{M}^T) \vec{z} = \vec{I} \quad (6)$$

and

$$E = 1 + \vec{z}_0^T \mathbf{M}^T \vec{z}, \quad (7)$$

where \vec{z}_0 is the initial seeding of each motif type at the start of the process. For example, consider the case where we have each node as being part of three cliques, where each clique contains three nodes (see Fig. 5), the elements of \vec{z}_0 are $(3, 0, 0, 0)^T$ and \vec{I} are $(0, 1, 2, 1)^T$. The first element of \vec{z}_0 is 3, as each node is a member of three cliques, and, as this is the seed configuration, the contagion has not spread to any other nodes, leaving all the other motif types zero. We simply count the number of active nodes in each motif for the elements of \vec{I} . Referring again to Fig. 5, types Z_2 and Z_4 both have one active node, and type Z_3 has two active nodes. We need to be careful not to double-count nodes, and as such, we set the first element of \vec{I} to zero. For the full derivation, please refer to Ref. [12]. Using this, we can now easily sweep through a parameter set to find the relationship between p , the initial probability of infection, and α , the probability of quarantine on the expected epidemic size under our mean-field view of the disease process. Looking at the qualitative behavior of the curves, we see from Fig. 9 that as we increase p , naturally, the expected epidemic size increases; however, when we increase α , we see that the average size of the outbreak decreases across all three network topologies that we consider. Moreover,

this effect is most pronounced for networks with larger cliques, as this network gives the quarantining behavior more opportunities to remove possible infection paths via our mean-field approximation. These results also hold for the complex-contagion approximation to the model, which is discussed in the next section. Please refer to Appendix A for the complex contagion approximation calculation for the expected cascade size calculation.

III. COMPLEX CONTAGION APPROXIMATION

The model described in Sec. IC is closely related to a SIR model, which allows the probability of infection to change as a function of infection attempts. In this related model, we do not keep track of isolated node states. Instead, we keep track of failed infection attempts on the susceptible nodes. Since we know that a contact tracing attempt preceded each infection attempt, we know that there has been an equal number of infection attempts and contact tracing attempts. In this sense, each infection attempt also carries a risk of isolation, and every attempt becomes less likely to yield an infected node. This is in contrast to the typical social complex contagion processes where each infection attempt makes it more likely for the next one to succeed.

We borrow the framework of the multitype branching processes for complex contagion as introduced in Ref. [12], where the infection state of the nodes characterizes motifs. Notably, the model is exactly the same apart from p_k as has been previously defined in Ref. [12], where the probability of adoption after k attempts is given by

$$p_k = 1 - (1 - p)(1 - \alpha)^{k-1}. \quad (8)$$

That is, the α parameter works exactly opposite to the contact tracing here: the larger the α value, the larger the probability that infection attempts beyond the first one are likely to succeed.

In the SIR process with contact tracing each isolation fails with probability $1 - \alpha$ and a node is not isolated after k attempts with probability $(1 - \alpha)^k$. If the person is not isolated, they have a probability of p being infected by an adjacent infected node. In total, the probability that a node gets infected by a neighbor after k attempts, given that it is not yet infected, is

$$\hat{p}_k = p(1 - \alpha)^k. \quad (9)$$

This probability describes exactly the opposite behavior to typical social complex contagion processes, where the probability of infection increases with the number of attempts. Suppose we do not track whether the susceptible node is quarantined or the infection has failed even though the node was not quarantined. In that case, we can follow the method and formulas given in Ref. [12] by simply replacing the probability p_k of Eq. 8 with \hat{p}_k from Eq. 9. In this picture, isolated and susceptible nodes are

i, j	m_{ij}
1, 1	$4p(1 - \alpha)$
1, 2	$2p(1 - \alpha)^2$
2, 1	$2p(1 - \alpha)(1 - p(1 - \alpha))$
3, 1	$p^2(1 - \alpha)^2$
4, 2	$p(1 - \alpha)^2$

TABLE II. Non-zero elements of the next-generation matrix $\mathbf{M}_{4 \times 4}$ in the complex contagion approximation for a 3-clique network. m_{ij} gives the expected number of Z_i cliques from a Z_j clique. As shown in Fig. 5.

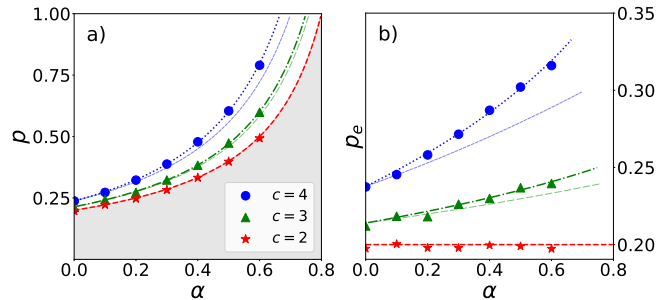


FIG. 10. Comparison of the mean-field approximation introduced in section Sec. II with the complex contagion approximation of Sec. III. Panels are similar to the panels of Fig. 6. Here, markers are the results of the simulations described in Sec. IIB 1. Our simulation results align with the bold curves, which are the results of the mean-field approximations of Sec. IIB 2. The thin curves are the result of the complex contagion approximation introduced in Sec. III, which deviates slightly more from the other mean-field approximation when α increases. The complex contagion approximation gives the lower bound of critical transmission probability for all values of α .

treated the same and put into the susceptible compartment. We are not explicitly tracking people in the Q compartment. However, rather we have made the probability of infection a function of the number of exposures as given by Eq. 9. In this approximation, we also retain the infected and quarantined nodes Q_I in the susceptible compartment S, which means that a Z_1 cannot make a Z_4 directly (Fig. 5).

Table II shows the non-zero elements of the next-generation matrix for a 3-clique network, and Fig. 10 shows the result of the complex contagion approximation when we set the spectral radius of the new next-generation matrix to unity. The results of this approximation are close to the simulations and the mean-field solution presented in Sec. IIB 2 when the quarantine probability α and clique size c are small. Larger α and c values will lead to underestimated epidemic threshold values for the infection probability p . This means that the complex contagion process acts as a lower bound for the full contact tracing process, and that the effects of contact tracing are larger than those of the complex contagion process. That is, the phenomenon of disease spreading

under contact tracing in networks with cliques can be understood to be analogous to social complex contagion but with the opposite and smaller effect. Intuitively, analogously to social complex contagion, this explains why it is crucial to consider contact tracing in network models that contain realistic group structures.

IV. CONCLUSION & DISCUSSION

In this paper, we show how to incorporate quarantining into a model of disease spread on social networks with a local group structure that is modeled with cliques. More precisely, we derive the impact of clique size as a function of contact tracing efficiency to the epidemic threshold and epidemic size. Using a deliberately simplified contact network structure, we illustrate how contact tracing can be more efficient than what would be predicted by models that assume a fully mixed population or a locally tree-like network structure. Moreover, when quarantining is less certain for lower α values, the outbreak size E decreases more by increasing the clique sizes. That is, contact tracing is more efficient in networks with more clustering than networks without clustering and the same average degree, i.e., the conventional epidemic models can underestimate the effectiveness of contact tracing. We show that disregarding group structure in contact tracing is analogous to disregarding group structure in models of complex contagion where previous exposures increase the chance of adoption/infection. This illustrates the possible benefits of contact tracing in real-world settings, especially in the early stage of disease spread, where quarantining limits the possible paths of infection that disease can take through a network. Our model is an idealized representation and therefore oversimplifies the complexities of disease transmission and contact tracing. In actual social situations, the implementation of contact tracing may vary across different groups within the network, resulting in strong effects on infection risk and threshold size. The networks we analyzed did not reflect real-world social contact networks, which are highly diverse. Further, our model integrates factors related to the timing of contact tracing and isolation into a single parameter α . In this simplification, contact tracing is always either entirely successful or entirely unsuccessful, while in reality, contact tracing could be partially successful such that the isolated individual passes on the infection to part of the contacts that would have been infected without any intervention. Further, there could be additional effects in networks with cliques that are affected by the timing. Further research is needed to understand how quarantining measures impact epidemics on more realistic contact networks with contact tracing and how outbreak sizes are

distributed in such settings.

Even more complications in the modeling will need to be considered if one wants to have a realistic model of individuals who are contact traced multiple times. If a susceptible person is traced twice, they could receive two separate notices of having been in touch with two separate infected individuals. Receiving multiple notices like this might reinforce the probability of the person isolating. On the other hand, the first tracing could fail, for example, due to the index case not being able to remember the contact. In this case, modeling the two tracing events as independent from each other is a reasonable assumption.

In summary, our results highlight the importance of considering realistic social network structures when modeling epidemics and interventions. Our model is deliberately simplistic, and it is used to isolate key insights. The key stylistic facts we extract are: (1) contact tracing is more efficient in social networks with groups than one would expect based on the tree-like models, (2) the effect of groups is larger if the groups are larger, and if the contact tracing is more efficient, and finally (3) SIR spreading under contact tracing can be approximately understood as a complex contagion process where multiple exposures reduce the infection probabilities.

CODE AVAILABILITY

The simulations and numerical computations used in this study are publicly available at [46].

ACKNOWLEDGEMENT

A. K. R. would like to thank Lasse Leskelä and Takayuki Hiraoka for the fruitful discussion during the preparation of this work. The simulations presented above were performed using computer resources within the Aalto University School of Science “Science-IT” project. A. K. R. and M. K. acknowledge funding from the project 105572 NordicMathCovid which is part of the Nordic Programme on Health and Welfare funded by NordForsk. This work was also supported by the Academy of Finland (349366, 353799). Moreover, This publication has emanated from research supported in part by a grant from Science Foundation Ireland under Grant numbers 18/CRT/6049, 16/IA/4470, 16/RC/3918 and 12/RC/2289 P2 (LAK and JPG) with co-funding from the European Regional Development Fund. For the purpose of Open Access, the author has applied a CC BY public copyright licence to any Author Accepted Manuscript version arising from this submission.

[1] D. Lewis, Why many countries failed at covid contact-tracing—but some got it right., *Nature* **588**, 384 (2020).

[2] Contact tracing: digital health on the frontline, *The Lancet. Digital Health* **2**, e561 (2020).

- [3] L. E. Smith, R. Amlôt, H. Lambert, I. Oliver, C. Robin, L. Yardley, and G. J. Rubin, Factors associated with adherence to self-isolation and lockdown measures in the uk: a cross-sectional survey, *Public Health* **187**, 41 (2020).
- [4] X. Wang, Z. Du, E. James, S. J. Fox, M. Lachmann, L. A. Meyers, and D. Bhavnani, The effectiveness of covid-19 testing and contact tracing in a us city, *Proceedings of the National Academy of Sciences* **119**, e2200652119 (2022).
- [5] S. Galea, R. M. Merchant, and N. Lurie, The mental health consequences of covid-19 and physical distancing: the need for prevention and early intervention, *JAMA internal medicine* **180**, 817 (2020).
- [6] A. J. Kucharski, P. Klepac, A. J. Conlan, S. M. Kissler, M. L. Tang, H. Fry, J. R. Gog, W. J. Edmunds, J. C. Emery, G. Medley, *et al.*, Effectiveness of isolation, testing, contact tracing, and physical distancing on reducing transmission of sars-cov-2 in different settings: a mathematical modelling study, *The Lancet Infectious Diseases* **20**, 1151 (2020).
- [7] N. J. Salkind, *Encyclopedia of educational psychology* (SAGE publications, 2008) pp. 150–152.
- [8] R. D. Luce and A. D. Perry, A method of matrix analysis of group structure, *Psychometrika* **14**, 95 (1949).
- [9] C. Stegehuis and T. Peron, Network processes on clique-networks with high average degree: the limited effect of higher-order structure, *Journal of Physics: Complexity* **2**, 045011 (2021).
- [10] S. L. Feld, The focused organization of social ties, *American journal of sociology* **86**, 1015 (1981).
- [11] E. Bokányi, E. M. Heemskerk, and F. W. Takes, The anatomy of a population-scale social network, arXiv:2211.15325 (2022).
- [12] L. A. Keating, J. P. Gleeson, and D. J. O’Sullivan, Multi-type branching process method for modeling complex contagion on clustered networks, *Physical Review E* **105**, 034306 (2022).
- [13] L. A. Keating, J. P. Gleeson, and D. J. O’Sullivan, A generating-function approach to modelling complex contagion on clustered networks with multi-type branching processes, arXiv:2212.00584 (2022).
- [14] D. Centola and M. Macy, Complex contagions and the weakness of long ties, *American journal of Sociology* **113**, 702 (2007).
- [15] A. K. Rizi, A. Faqeeh, A. Badie-Modiri, and M. Kivelä, Epidemic spreading and digital contact tracing: Effects of heterogeneous mixing and quarantine failures, *Physical Review E* **105**, 044313 (2022).
- [16] T. Hiraoka, A. K. Rizi, M. Kivelä, and J. Saramäki, Herd immunity and epidemic size in networks with vaccination homophily, *Physical Review E* **105**, L052301 (2022).
- [17] B. Karrer and M. E. Newman, Random graphs containing arbitrary distributions of subgraphs, *Physical Review E* **82**, 066118 (2010).
- [18] N. C. Wormald *et al.*, Models of random regular graphs, *London Mathematical Society Lecture Note Series* , 239 (1999).
- [19] B. Bollobás, Random graphs, in *Modern graph theory* (Springer, 1998) pp. 215–252.
- [20] E. Kenah and J. C. Miller, Epidemic percolation networks, epidemic outcomes, and interventions, *Interdisciplinary perspectives on infectious diseases* **2011** (2011).
- [21] A. Badie-Modiri, A. K. Rizi, M. Karsai, and M. Kivelä, Directed percolation in random temporal network models with heterogeneities, *Physical Review E* **105**, 054313 (2022).
- [22] A. Badie-Modiri, A. K. Rizi, M. Karsai, and M. Kivelä, Directed percolation in temporal networks, *Physical Review Research* **4**, L022047 (2022).
- [23] M. Newman, *Networks* (Oxford university press, 2018).
- [24] M. E. Newman, Random graphs with clustering, *Physical review letters* **103**, 058701 (2009).
- [25] J. C. Miller, Percolation and epidemics in random clustered networks, *Physical Review E* **80**, 020901 (2009).
- [26] J. P. Gleeson, S. Melnik, and A. Hackett, How clustering affects the bond percolation threshold in complex networks, *Physical Review E* **81**, 066114 (2010).
- [27] F. Ball, D. Sirl, and P. Trapman, Analysis of a stochastic sir epidemic on a random network incorporating household structure, *Mathematical Biosciences* **224**, 53 (2010).
- [28] E. Coupechoux and M. Lelarge, How clustering affects epidemics in random networks, *Advances in Applied Probability* **46**, 985 (2014).
- [29] P. Mann, V. A. Smith, J. B. Mitchell, and S. Dobson, Random graphs with arbitrary clustering and their applications, *Physical Review E* **103**, 012309 (2021).
- [30] R. van der Hofstad, J. S. van Leeuwen, and C. Stegehuis, Hierarchical configuration model, arXiv:1512.08397 (2015).
- [31] C. Stegehuis, R. Van Der Hofstad, and J. S. Van Leeuwen, Epidemic spreading on complex networks with community structures, *Scientific reports* **6**, 1 (2016).
- [32] J. C. Miller, Spread of infectious disease through clustered populations, *Journal of the Royal Society Interface* **6**, 1121 (2009).
- [33] S. Melnik, A. Hackett, M. A. Porter, P. J. Mucha, and J. P. Gleeson, The unreasonable effectiveness of tree-based theory for networks with clustering, *Physical Review E* **83**, 036112 (2011).
- [34] R. Pastor-Satorras, C. Castellano, P. Van Mieghem, and A. Vespignani, Epidemic processes in complex networks, *Reviews of modern physics* **87**, 925 (2015).
- [35] M. E. Newman, Spread of epidemic disease on networks, *Physical review E* **66**, 016128 (2002).
- [36] D. Zhang and T. Britton, Epidemic models with digital and manual contact tracing, arXiv:2211.12869 (2022).
- [37] L. Ferretti, C. Wymant, M. Kendall, L. Zhao, A. Nurtay, L. Abeler-Dörner, M. Parker, D. Bonsall, and C. Fraser, Quantifying sars-cov-2 transmission suggests epidemic control with digital contact tracing, *Science* **368**, eabb6936 (2020).
- [38] M. E. J. Newman, Message passing methods on complex networks, *Proceedings of the Royal Society A: Mathematical, Physical and Engineering Sciences* **479**, 20220774 (2023).
- [39] O. Diekmann, H. Heesterbeek, and T. Britton, *Mathematical tools for understanding infectious disease dynamics*, Vol. 7 (Princeton University Press, 2013).
- [40] E. Kenah and J. M. Robins, Second look at the spread of epidemics on networks, *Physical Review E* **76**, 036113 (2007).
- [41] M. Li, R.-R. Liu, L. Lü, M.-B. Hu, S. Xu, and Y.-C. Zhang, Percolation on complex networks: Theory and application, *Physics Reports* **907**, 1 (2021).
- [42] S. N. Dorogovtsev, A. V. Goltsev, and J. F. Mendes, Critical phenomena in complex networks, *Reviews of Modern Physics* **80**, 1275 (2008).

- [43] H. Caswell, *Matrix population models*, Vol. 1 (Sinauer Sunderland, 2000).
- [44] O. Diekmann, J. A. P. Heesterbeek, and J. A. J. Metz, On the definition and the computation of the basic reproduction ratio R_0 in models for infectious diseases in heterogeneous populations, *Journal of Mathematical Biology* **28**, 365 (1990).
- [45] A. F. Brouwer, Why the spectral radius? an intuition-building introduction to the basic reproduction number, *Bulletin of Mathematical Biology* **84**, 96 (2022).
- [46] Github repository, <https://github.com/k-rizi/Contact-Tracing-On-Clique-Networks>.
- [47] R. S. Varga, *Matrix iterative analysis*, Vol. 27 (Springer Science & Business Media, 1999).

Appendix A: Expected epidemic size for the complex-contagion process

We can calculate the expected epidemic size for a multi-type branching process in the sub-critical regime, as explained in Sec. II B 3. Here, we examine the expected epidemic sizes for the complex-contagion process. To do this, we need only to replace the next-generation matrix from the mean-field description in Sec. II B 2 with that of the complex-contagion in Eqs. 6 and 7. As with the results from Sec. II B 3, we find good agreement when comparing the resulting curves for the expected epidemic (cascade) size, E , to simulation results in Fig. 11. When examining the qualitative behavior of the curves for expected epidemic size, we see from Fig. 11 that as we increase p , as expected, the expected epidemic size increases. However, when we increase α , we see that each network's average outbreak size decreases. Moreover, this effect is most pronounced for networks with larger cliques, as this network gives the quarantining behavior more opportunities to remove possible infection paths via the complex-contagion approximation to the process.

Appendix B: Reproduction number and the next-generation matrix

We will next give additional details on using the leading eigenvalue of the \mathbf{M} matrix as the reproduction number R_e . There are two specific issues that were only briefly discussed in the main text: why does the leading eigenvalue of the reducible matrix \mathbf{M} tell about the critical behavior, and why can the leading eigenvalue be interpreted as R_e ?

The argument for the leading eigenvalue of the reducible matrix \mathbf{M} determining the criticality is very similar to the one made in Sec. IV A 2 of Ref. [12]. We can divide the transitions between Z states into two categories: ones that describe changes within a clique and ones that describe the infection arriving in a clique that previously only had susceptible nodes. The transitions within cliques form a directed acyclic graph (DAG), because the SIR+Q process always moves in one direction,

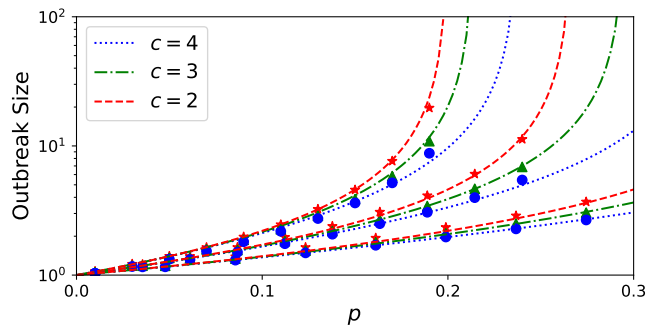


FIG. 11. Outbreak size in the sub-critical regime as a function of p across the three network structures, while taking into account the influence of isolation probability α . Nine curves are grouped into three sets (from left to right) according to their isolation probabilities, with each set containing $\alpha = 0.0$, $\alpha = 0.25$, and $\alpha = 0.5$. These groupings demonstrate the influence of α on outbreak size in the sub-critical regime. Increasing α or clique size reduces the outbreak size, as calculated by Eq.6 and Eq.7 using the next-generation matrix from mean-field approximation found in Sec. III. Markers represent the results of 50,000 simulations, while dotted lines depict the results of the mean-field calculations presented in Sec. II B 3.

i.e., from susceptible to infected or removed or from infected to removed. DAGs can always be put into upper (or lower) triangular form. Every motif that has at least one susceptible and one infected node will have a transition to the Z_1 state, which has one infected node in an otherwise susceptible clique. We can permute the matrix \mathbf{M} in a way that we collect these motifs to a block \mathbf{B}_1 . These motifs form a block that is strongly connected because Z_1 is the root of the DAG and the block is thus irreducible. The remaining states are still in the triangular form where each motif forms its own block \mathbf{B}_i , so in total we have the matrix in a normal form. Further, the motifs that do not belong to the block \mathbf{B}_1 are dead ends in the process as they cannot produce any offspring with infected nodes.

The method described above can always be used to write the reducible matrix \mathbf{M} in its normal form such that blocks \mathbf{B}_i fill the upper triangle part of it. Since \mathbf{M} is non-negative, the spectrum of \mathbf{M} is the union of the spectra of the \mathbf{B}_i [47]. Here the B_i has zero eigenvalues for $i \neq 1$, and the largest eigenvalue of \mathbf{M} , i.e., the Perron root, is the same as the largest eigenvalue of \mathbf{B}_1 which is an irreducible matrix. Given that we initialize our spreading process sparsely such that there are only Z_1 motifs in the network in the beginning (in addition to the fully susceptible ones we do not track), the long-term dynamics will always be governed by the leading eigenvalue of \mathbf{B}_1 (and therefore \mathbf{M}) [12].

The R_e correspondence to the leading eigenvalue might initially seem non-intuitive, considering that some transitions create multiple infected nodes at one step. This indicates that one needs to multiply the effects of transi-

tions by the number of newly infected nodes in them to compute the expected number of newly infected nodes a typical infected node produces. However, this is not necessary. A key observation here is that the number of Z_1 motifs is directly proportional to the number of infected nodes in the network. Every time a node is infected, it will create $n_c - 1$ of new Z_1 motifs, where n_c is the number of cliques each node belongs to. In the next time step those motifs transition into one of the other motif types and the infected individuals become removed so the number of Z_1 motifs is always updated to be $n_c - 1$ times the number of infected nodes. That is, at time step t , the number of infected nodes is $I^t = Z_1^t / (n_c - 1)$, where Z_1^t is the number of motifs Z_1 at time t . Given that we are at the steady state, Z^t is the leading eigenvector, i.e., $Z^{(t+1)} = MZ^t = \lambda Z^t$, and $Z_1^{(t+1)} = \lambda Z_1^t$, which means that $I^{(t+1)} = \lambda I^t$.

Appendix C: Automatic generation of the next-generation matrices

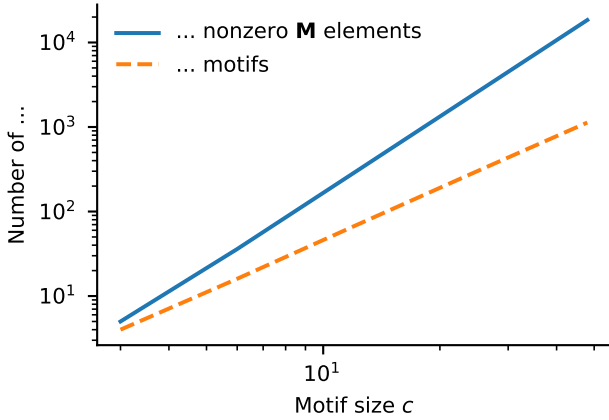


FIG. 12. Number of motifs and the number of nonzero elements of \mathbf{M} for given clique size c .

We show how the next-generation matrix can be constructed for any size of c by an algorithm described here. The construction by going through every motif and considering what are the transitions and expected values leading out of that motif. That is, we go one motif at a time, starting from the one that has only a single infected node and the rest of the nodes susceptible, construct the motifs one time step away from that motif and the expected number of new motifs produced.

We use here notation where motifs are defined by the number of nodes in each compartment in them, i.e., we define motif $Z = (n_S, n_I, n_R)$ as one that has n_S susceptible nodes, n_I infected nodes, and n_R removed (recovered or quarantined) nodes. Initially, we start with the motif

$$Z_1 = (c - 1, 1, 0).$$

We process the motifs one at a time, with the following rules. If the motif Z_i has no infected nodes, we do nothing. If it has one or more infected nodes, we then create transitions to new motifs $Z_j = (n_S + \delta n_S, n_I + \delta n_I, n_R + \delta n_R)$, for all $\delta n_I \in \{1, \dots, n_S\}$, $\delta n_R \in \{0, \dots, n_S - \delta n_I\}$, and $\delta n_S = -\delta n_I - \delta n_R$. If those new motifs have not been processed before, they are added to a queue for being processed.

The transition probabilities m_{ji} can then be computed for $j \neq 1$ by

$$\binom{n_S}{\delta n_I} \binom{n_S - \delta n_I}{\delta n_R} p(n_I)^{\delta n_I} (1 - p(n_I))^{n_S + \delta n_S} \cdot \alpha^{\delta n_R} (1 - \alpha)^{n_S - \delta n_R}, \quad (\text{C1})$$

where the probability of n_I nodes causing a node to get infected is

$$p(n_I) = \sum_{k=0}^{n_I-1} (\alpha - 1)^k (1 - p)^k p. \quad (\text{C2})$$

The element m_{1i} can be computed by

$$m_{1i} = (n_c - 1) \sum_{j \neq 1} \delta n_I(j, i) m_{ji}, \quad (\text{C3})$$

where the value $\delta n_I(j, i)$ is the value of δn_I in the transition from Z_i to Z_j .

This procedure will yield sparse matrices \mathbf{M} matrices, where the size of the matrix and the number of non-zero elements grow as shown in Fig. 12. This process allows us to automatically generate the mean matrices for any clique size we wish to examine efficiently.

Next-generation matrices for 4-cliques

Fig. 13 shows the life stages of a 4-clique. For this case, the next-generation matrix according to the mean-field and complex contagion approximations are given by Table III and Table IV respectively.

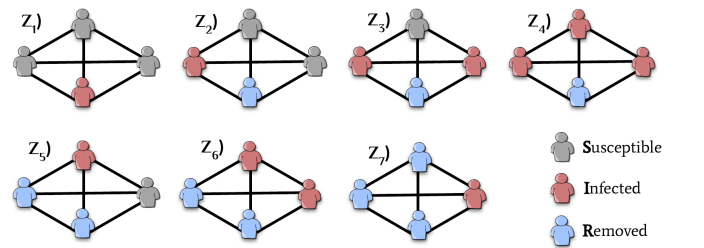


FIG. 13. Life stages or diffusion patterns of a 4-clique. Similar to Fig. 5 for a 3-clique. We can generate the next-generation matrix for any clique size with our code introduced in Sec. C.

i, j	m_{ij}
1, 1	$3p(-\alpha n_c + \alpha + n_c - 1)$
1, 2	$2p(-\alpha n_c + \alpha + n_c - 1)$
1, 3	$p(1 - \alpha)(n_c - 1)((\alpha - 1)(p - 1) + 1)$
1, 5	$-p(\alpha - 1)(n_c - 1)$
2, 1	$-3p(\alpha - 1)^3(p - 1)^2$
3, 1	$3p^2(\alpha - 1)^3(p - 1)$
4, 1	$-p^3(\alpha - 1)^3$
5, 1	$-6\alpha p(\alpha - 1)^2(p - 1)$
5, 2	$-2p(\alpha - 1)^2(p - 1)$
6, 1	$3\alpha p^2(\alpha - 1)^2$
6, 2	$p^2(\alpha - 1)^2$
7, 1	$3\alpha^2 p(1 - \alpha)$
7, 2	$2\alpha p(1 - \alpha)$
7, 3	$p(1 - \alpha)((\alpha - 1)(p - 1) + 1)$
7, 5	$p(1 - \alpha)$

TABLE III. Non-zero elements of the next-generation matrix \mathbf{M} for a 4-clique network as explained in Sec. II B 2. m_{ij} gives the expected number of Z_i cliques from a Z_j clique, as shown in Fig. 13. n_c is the number of cliques of size $c = 4$ which for an r -regular c -clique satisfies the identity $n_c(c - 1) = r$.

i, j	m_{ij}
1, 1	$3p(n_c - 1)$
1, 2	$-2(n_c - 1)((\alpha - 1)(p - 1) - 1)$
1, 3	$(n_c - 1)((\alpha - 1)^3(p - 1)^2 + 1)$
1, 5	$(n_c - 1)((\alpha - 1)^2(p - 1) + 1)$
2, 1	$3p(p - 1)^2$
3, 1	$3p^2(1 - p)$
4, 1	p^3
5, 2	$2(1 - \alpha)(p - 1)((\alpha - 1)(p - 1) - 1)$
6, 2	$(\alpha p - \alpha - p)^2$
7, 3	$(\alpha - 1)^3(p - 1)^2 + 1$
7, 5	$(\alpha - 1)^2(p - 1) + 1$

TABLE IV. Non-zero elements of the next-generation matrix \mathbf{M} in the complex contagion approximation for a 4-clique network. m_{ij} gives the expected number of Z_i cliques from a Z_j clique.